ACS APPLIED MATERIALS & INTERFACES

www.acsami.org

Research Article

# Lotus Leaf-Inspired Breathable Membrane with Structured Microbeads and Nanofibers

Shuo Shi, Chuanwei Zhi, Shuai Zhang, Jieqiong Yang, Yifan Si, Yuanzhang Jiang, Yang Ming, Kin-tak Lau, Bin Fei, and Jinlian Hu*

Cite This: *ACS Appl. Mater. Interfaces* 2022, 14, 39610−39621



**ABSTRACT:** Electrospinning is a feasible technology to fabricate nanomaterials. However, the preparation of nanomaterials with controllable structures of microbeads and fine nanofibers is still a challenge, which hinders widespread applications of electrospun products. Herein, inspired by the micro/nanostructures of lotus leaves, we constructed a structured electrospun membrane with excellent comprehensive properties. First, micro/nanostructures of membranes with adjustable microbeads and nanofibers were fabricated on a large scale and quantitatively analyzed based on the controlling preparation, and their performances were systematically evaluated. The deformation of diverse polymeric solution droplets in the electrospinning process under varying electric fields was then simulated by molecular dynamic simulation. Finally, novel fibrous membranes with structured sublayers and controllable morphologies were designed, prepared, and compared. The achieved structured membranes demonstrate a high water vapor transmission rate (WVTR) > 17.5 kg/(m$^2$ day), a good air permeability (AP) > 5 mL/s, a high water contact angle (WCA) up to 151°, and a high hydrostatic pressure of 623 mbar. The disclosed science and technology in this article can provide a feasible method to not only adjust micro/nanostructure fibers but also to design secondary multilayer structures. This research is believed to assist in promoting the diversified development of advanced fibrous membranes and intelligent protection.

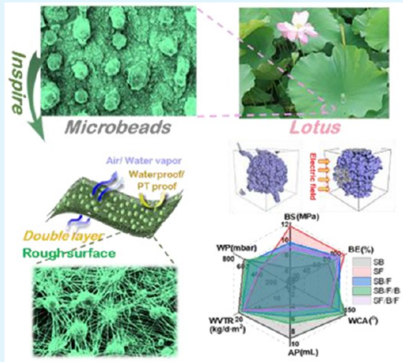


**KEYWORDS:** *lotus leaf, controllable electrospinning, biomimetic, waterproof breathable, fibrous membrane*



## 1. INTRODUCTION

Biological materials such as lotus leaves, polar bear hairs, and spider webs have abundant interesting properties.[1] The leaves of lotus have various micro/nanostructures, so they demonstrate excellent hydrophobicity, good water repellency, and self-cleaning characteristics.[2] As hairs of polar bears possess microhollow structures, they have a super thermal insulation function.[3] Spider webs have high toughness, so they are used to capture insects.[4,5] Bionic technology inspired by the phenomena of these biological materials has achieved significant progress in various fields. However, considering the feasibility of fabricating processes, many current methods cannot prepare biomimetic structures on a large scale due to complex preparation processes and rigorous processing requirements.[6] Therefore, developing a feasible approach to construct biomimetic structures is significant and valuable.

Electrospinning technology has a long history, and various electrospun products have been widely used in high-efficiency catalysis, energy harvesters, smart wearables, and other high-added-value fields.[7−9] Significantly, besides these applications, electrospun technology has shown an increasing trend for the application of protective membranes.[1,10] Protective properties refer to the membrane that has the characteristic of protection against virus aerogel, toxic particles, liquid splashes, etc.[11−14] The global market size of medical protective clothing was valued at USD 12.48 billion in 2019, and it is predicted to reach up to USD 34.31 billion in 2027.[15] Additionally, with the ravages of Covid-19 throughout the world, the demand for protective membranes is showing a blowout growth.[16−18] Traditional protective membranes are mainly divided into two categories. One is membranes with a medical protection function, which are generally used in surgical masks and medical protective clothing;[14,19−22] the other is membranes with a waterproof-breathable function, which are usually used in the application of mountaineering jackets and water directional transport clothing.[23−29] However, medical protection membranes are mainly prepared by melt-blown and melt-spun hydrophobic polypropylene (PP),[30,31] and the largest market share of waterproof-breathable clothing is currently that produced with the bidirectional stretched PTFE membrane.[32] These two traditional manufacturing processes involve high-temperature

Received: June 24, 2022
Accepted: August 11, 2022
Published: August 18, 2022

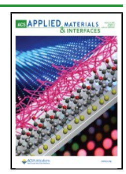




https://doi.org/10.1021/acsami.2c11251
*ACS Appl. Mater. Interfaces* 2022, 14, 39610−39621

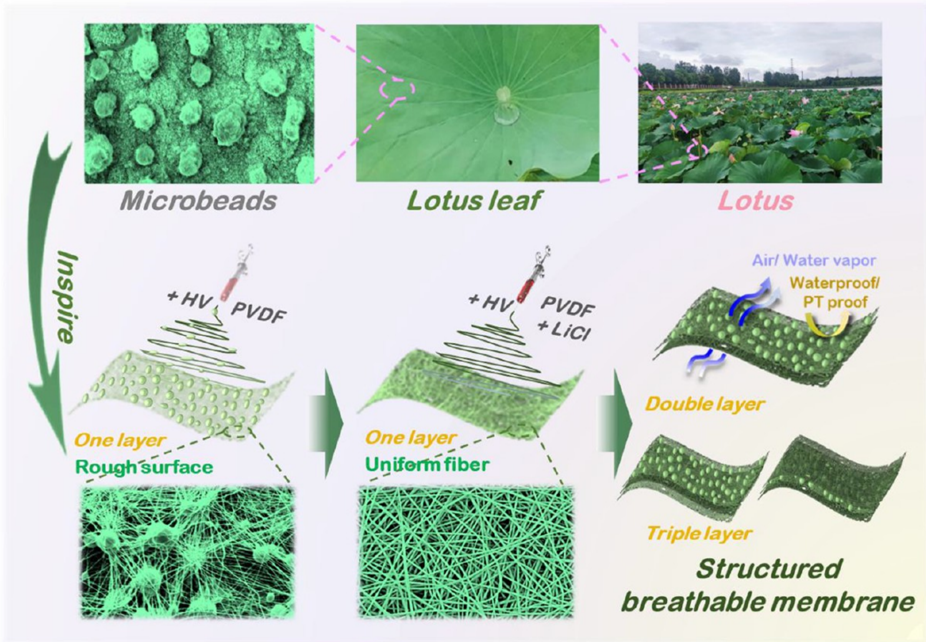


**Figure 1.** Microstructures of a lotus leaf and the design of electrospun membranes with structured layers with controllable microbeads and nanofibers.

**Table 1. Controlling Parameters and Formulas Used to Fabricate Structured Electrospun Membranes**[a]

| P / S | V (kV) | C (%) | Toc (cm) | FS (mL/h) | LiCl (%) |
|---|---|---|---|---|---|
| SB | 25 | 15 | 15 | 0.3 | 0 |
| SF | 25 | 20 | 15 | 0.3 | 0.2 |
| SB/SF | 25 | 15→20 | 15 | 0.3 | 0→0.2 |
| SB/SF/SB | 25 | 15→20→15 | 15 | 0.3 | 0→0.2→0 |
| SF/SB/SF | 25 | 20→15→20 | 15 | 0.3 | 0.2→0→0.2 |

[a]P, controlling parameters; S, samples; SB, sample with microbeads; SF, sample with all fine nanofibers; SB/SF, sample with a half layer of a microbead-based membrane and a half layer of a fine nanofiber-based membrane; SB/SF/SB, sample with a sandwich structure where the middle is a nanofiber-based layer and the two outside layers are microbead-based; SF/SB/SF, sample with a sandwich structure where the middle is a microbead-based layer and the two outside layers are nanofiber-based; →, indicated switching the formula.

processing; therefore, energy consumption in manufacturing processes is relatively heavy.[33−35] Meanwhile, high-temperature processes do not favor the addition of active materials and functional nanoparticles. Therefore, developments and new solutions to problems of fabricating protective membranes are urgently needed.

At present, researchers have gradually focused on developing novel micro/nanotechnology via advanced electrospinning. Fibers prepared based on electrospinning technology have the characteristics of a large specific surface area.[36−38] Meanwhile, the simple processing process and easy reconfiguration of electrospun equipment endow electrospun micro/nanoproducts with diverse functions, which are beneficial to the manufacture of advanced protective membranes.[39−43] Therefore, electrospun membranes have great potential application in many devices due to their high-efficiency filtration, good breathability, waterproofness, windproofness, etc.[44−50] However, the corresponding disadvantages of electrospun products are also obvious. Thinner fibers lead to greater resistance to fluid movement, and the surface of the constructed membrane is relatively flat, making it difficult to control the contact angle between the membrane and water. Researchers have made various attempts to overcome these problems. For example, inspired by the structure of the lotus leaf, Jiang et al. reported a methodology to construct a superhydrophobic membrane vis polystyrene solution, and the prepared membrane with microbeads displayed a high WCA.[2] This research has great significance for subsequent bionic structure research. However, other comprehensive properties of the fibrous membranes were not evaluated in this study. For electrospun products applied in different environments, it is still a challenge to manage the comprehensive properties of micro/nanoproducts through designing integrated micro/nanostructures. Investigation of


https://doi.org/10.1021/acsami.2c11251
ACS Appl. Mater. Interfaces 2022, 14, 39610−39621

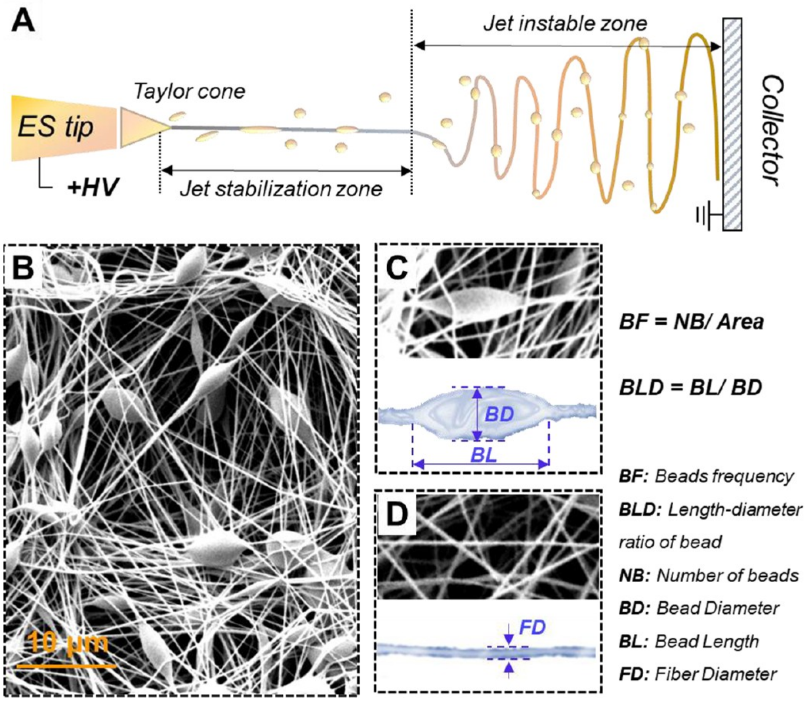


**Figure 2.** Quantitative definition with regards to characteristics of microbeads and nanofibers. (A) Schematic diagram of the electrospun process with a typical Taylor cone, jet stabilization zone, and jet unstable zone. (B) Typical SEM picture of the electrospun membrane with microbeads and nanofibers. (C, D) Definitions of quantitative values of microbeads and nanofibers.

these problems and corresponding solutions can greatly promote electrospun applications.

Inspired by the lotus leaf structures, in this study, we constructed an interesting structure with controllable microbeads and fine nanofibers and investigated the overall performances of prepared membranes. In addition, we built a quantitative method and molecule dynamic simulation to investigate the effects of several parameters, such as the applied voltage ($V$), the distance between the tip and the collector (Toc), the feed speed (FS), the polymer solution concentration ($C$), and the conductivity of the polymer solution, on the electrospinning process, the morphology of the fiber, and the comprehensive properties of the final products. Subsequently, we designed, prepared, and compared the comprehensive properties of structured microbead/nanofiber membranes with multiple layers. The results show that structured membranes with microbeads/nanofibers and secondary layers display a better comprehensive property, promoting a wide range of applications in terms of biomimetic membranes. Furthermore, the approaches used in this article have strong expansibility and inspiration for the development of electrospun technology and materials science.

## 2. EXPERIMENTAL SECTION

**2.1. Materials and Fabricating Processes.** Polyvinylidene fluoride (PVDF), lithium chloride (LiCl), and dimethylformamide (DMF) were purchased from the Shanghai Aladdin Bio-Chem Technology Co., Ltd. All chemicals used in experiments were without any purification and pretreatment. Structured fibrous membranes were constructed by an electrospinning system provided by the Kato Tech Co., Ltd. All electrospun experiments were conducted in a standard textile lab. Polymer solutions with various formulas and controlling parameters to produce structured fibrous membranes were shown in Table S1. Fibrous membranes with controllable characteristics of microbeads and nanofibers have been adjusted by different parameters. Multiple layers of membranes with microbead-based layers and fine nanofiber-based layers were fabricated according to Figure 1 and Table 1.

**2.2. Characterization.** The molecular structure of prepared fibrous membranes was evaluated by a PerkinElmer Fourier transform infrared spectrometer (FT-IR) (model 100 instrument, Waltham, MA, USA). Micro/nanostructures and element mapping of fabricated fibrous membranes were measured by a scanning electron micrograph (SEM) (TESCAN VEGA3, from Brno, Czech Republic). Samples were coated with gold first and then placed into the SEM machine for analysis. Stress−strain curves of fabricated samples were measured by an Instron 4466 with the sample in a rectangular shape of 50 mm × 10 mm. The speed of the loading rate during tests was set at 200 mm/min. The hydrostatic pressure of fibrous nanomembranes was evaluated by the FX 3000 Hydro Tester at 25 ± 2 °C. The increasing gradient rate of water pressure was kept at 150 mbar. The air permeability of different fibrous membranes was evaluated by an SDL air permeability instrument. Water contact angles of fabricated fibrous nanomembranes were measured by an optical video contact angle instrument produced from Lunderskov, Denmark. The water droplet used was 5 $\mu$L at room temperature.

The water vapor transmission rate (WVTR) of electrospun membranes was measured by a constant temperature and humidity chamber (model HD-E702-100-4, Haida International Equipment, Dongguan, China). Equation 1 was used to calculate WVTR. Data from different testing times were collected.

$$\mathrm{WVTR} = (M_0 - M_1)/ST \tag{1}$$

Where $M_0$ and $M_1$ (g) are the weight of containers with the sample at the initial and final state, $S$ (m$^2$) is the area of the cup, and $T$ (h) is the testing time.

*Molecular Dynamics of the Electrospinning Process.* To understand the applied high voltage and the concentration of polymeric solutions in the electrospun process and achieved electrospun membrane, we investigated the deformation of a droplet of PVDF in DMF solvent under varying conditions using *BIOVIA Materials Studio*. The quantum chemical calculations and deformation length ratios in different directions based on molecular dynamics simulation were

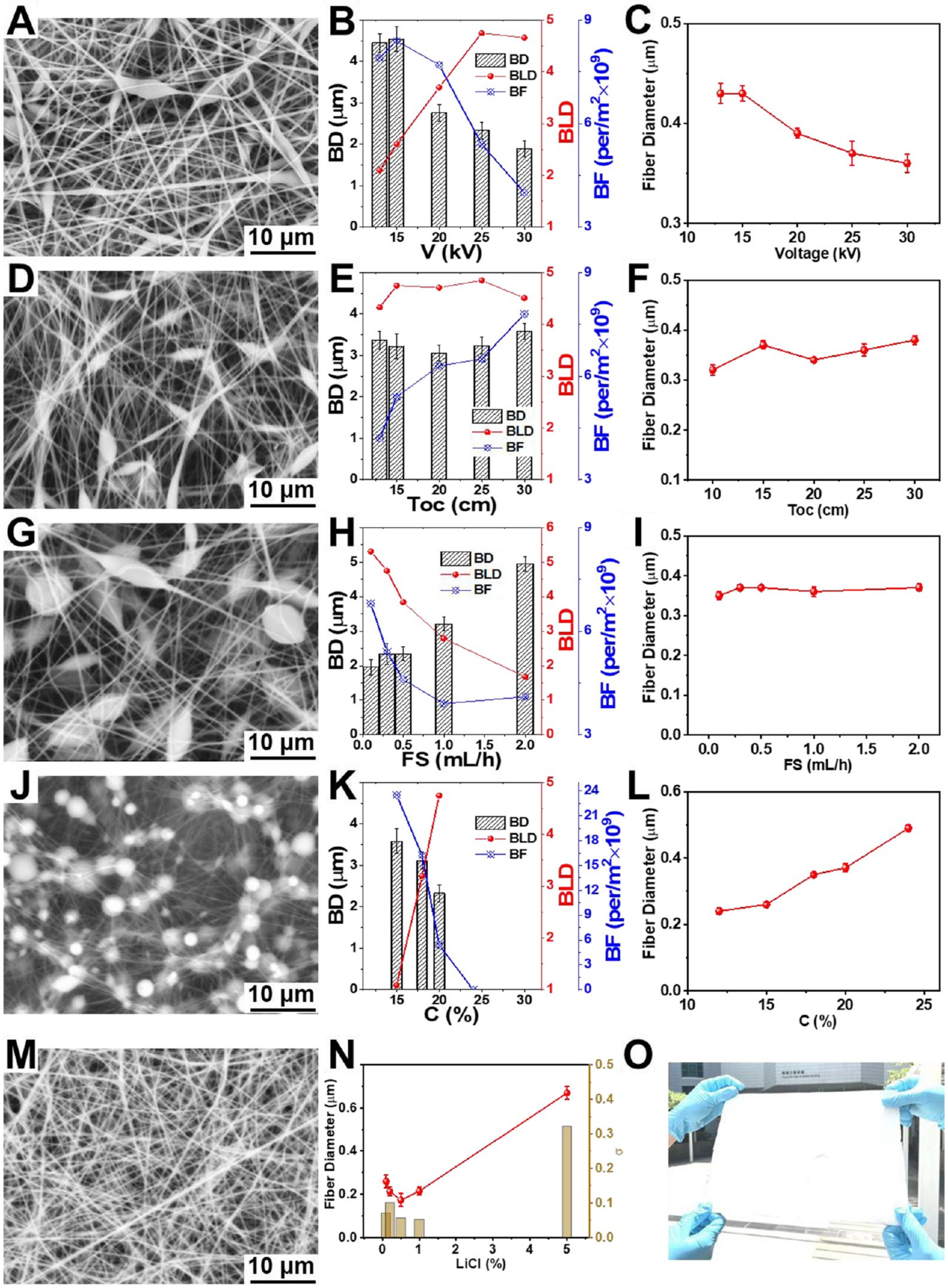


Figure 3. Factors in microbeads and nanofibers of electrospun membranes. (A−C) Typical SEM picture and quantitative characteristics of microbeads and nanofibers over V; (D−F) typical SEM picture and quantitative characteristics of microbeads and nanofibers over Toc; (G−I) typical SEM picture and quantitative characteristics of microbeads and nanofibers over FS; (J−L) typical SEM picture and quantitative characteristics of microbeads and nanofibers over C; (M, N) typical SEM picture and quantitative characteristics of nanofibers over LiCl; (O) optical picture of the fabricated electrospun membrane.

studied and evaluated. Briefly, the PVDF droplet was first optimized by Geometry Optimization, and then the equilibrium geometries were built; last, the varying electric fields were applied by the Force field method in *COMPASS*.[51−53] The length deformation rations of droplets in the three-dimensional directions were calculated and analyzed.

## 3. RESULTS AND DISCUSSION

The micro/nanostructures play an important role in the properties of materials, and hence they determine the applications of materials. For electrospun products, the fiber diameter and distribution as well as the characteristics of beads have a great impact on the comprehensive properties of final products, such as mechanical property, air permeability, water vapor permeability, water contact angle, etc. Theoretically, micro/nanostructures of electrospun products can be managed by operating parameters and intrinsic characteristics of polymeric solutions. In this section, all factors including the applied voltage, the distance between tip and collector, the feed speed, the concentration of polymer solution, and the content of additives (LiCl) were systemically investigated during the electrospinning process. Based on the investigation of controllable morphology, we further prepared a variety of fibrous membranes with multiple functional structured sublayers as shown in Figure 1. Meanwhile, quantitative definition (Figure 2) and dynamic molecule simulation of the electrospinning process to microbeads and nanofibers, including the bead diameter (BD), the length to diameter ratio of beads (BLD), beads frequency (BF), as well as the fiber diameter (FB) and its distribution. Significantly, these quantitative analyses and dynamic simulations are first systematically studied, and detailed discussions are provided in the following sections.

**3.1. Construct Electrospun Membranes with Controllable Micronanomorphologies.** Adjusting microbeads and nanofibers can manage the roughness of the electrospun membranes, so that the hydrophilic/hydrophobic characteristics, air permeability, and water vapor transmission rate of the fibrous membrane can be controlled. Diverse influences of the applied voltage (*V*), the distance between tip to the collector (Toc), the feed speed (FS), the solution concentration (*C*), and the contents of LiCl on the morphologies of microbeads and nanofibers on electrospinning were systematically investigated. Specifically, we use the control variable method to adjust the parameters. For example, when we investigate the influence between *V* and electrospinning, the other parameters, such as Toc, FS, and *C*, were kept at fixed values. The detailed parameters used in the experiment are provided in Table S1. Corresponding results are shown in Figure 3.

Overall, operating parameters and solution properties, such as *V*, Toc, FS, *C*, and the content of LiCl significantly impact the BD, BLD, BF, and FD of the fibrous membrane. Microbeads and fine nanofibers were well managed via them. Specifically, with the increase in *V*, the BD shows a notable decreasing trend, from about 4.5 $\mu$m at 13 kV to approximately 1.9 $\mu$m at 30 kV (Figures 3A−C and Figure S1); BLD shows a rapid linear increasing trend from 2.1 to 4.8 with the voltage change from 13 to 25 kV, then BLD tends to a steady state; BF displays a gradual decreasing trend from $7.9 \times 10^9$ per/m$^2$ to $4.0 \times 10^9$ per/m$^2$ with the increase in *V*. At the same time, FD shows a regular change with the increase in *V*, it drops from 0.43 $\mu$m at 13 kV to 0.36 $\mu$m at 30 kV. On the contrary, Toc does not significantly impact on features of microbeads (Figure 3D−F and Figure S2). With the gradual increase in the Toc, changes in BD (3.4−3.6 $\mu$m) and BLD (4.3 ∼ 4.8) are slight. However, BF shows an increasing trend from $4.2 \times 10^9$ per/m$^2$ at 10 cm to $7.8 \times 10^9$ per/m$^2$ with the Toc. This phenomenon may relate to the characteristic of the electrospinning process. A typical electrospun process can be divided into two sections, meaning a jet stabilization zone and a jet instability area (Figure 2A). Therefore, when the Toc increases, the unstable zone may increase, leading to the factor that the BF of the electrospun membrane increases.

Meanwhile, FS and C have significant effects on the morphology of the electrospun membrane. With the gradual increase in the FS, both BF and BLD show gradual decreasing trends from $6.8 \times 10^9$ per/m$^2$ to $4.1 \times 10^9$ per/m$^2$, and from 5.3 to 1.7, respectively; meanwhile, BD showed an increasing trend, increasing from 2.0 $\mu$m to around 5.0 $\mu$m (Figure 3G−I and Figure S3). Interestingly, the increase in the concentration of the polymer solution significantly affects the formation of nanofibers (Figure 3J−L and Figure S4). Particularly, electrospun nanofibers are difficult to be directly prepared when the concentration of the polymer solution is lower than 15%; all fibers prepared contain microbeads when the concentration is lower than 20%, while microbeads disappear and fine nanofibers are constructed when the concentration is higher at 24% (Figure 3K, L and Figure S4). A large amount of solvent favors forming a spherical shape of polymer solution droplet so that microbeads are constructed when the solution is at low concentrations; the interaction between the polymer chain and the solvent surpasses the tendency of the solvent liquid to become a spherical shape when the concentration increases, and thus fine nanofibers can be obtained. Therefore, through investigation, we found that controlling factors *V* and *C* have a greater influence on morphologies of microbeads and nanofibers compared with factors of Toc and FS. It is worth noting that the increase in the polymeric concentration of the polymer solution leads to an increase in the nanofiber diameter, theoretically decreasing the specific surface area of electrospun materials. Additionally, the increase in polymeric concentration easily causes the blockage of the needle and the termination of the electrospinning process. So, developing a novel method to manage the morphology of the electrospun membrane is important.

Theoretically, the electrospun process is a solidification process of the polymer solution driven by the electric field.[54] Thus, the jet process of the electrospinning can be adjusted if the conductivity of the polymer solution is changed. LiCl is an interesting inorganic salt that not only has good solubility in dimethylformamide (DMF) but also can enhance the conductivity of the polymer solution.[55] We studied the effect of LiCl on the electrospinning process of polyvinylidene fluoride (PVDF) (Figure 3M, N and Figure S5), and a large-scale image of the prepared electrospun membrane is given in Figure 3O. The results revealed that the electrospinning process of PVDF was optimized by adding a small amount of LiCl (0.1%), meaning that microbeads disappeared and fine nanofibers with a narrow distribution were constructed. Interestingly, the FD showed a trend of decreasing first from 0.26 to 0.17 $\mu$m and then increasing from 0.17 to 0.67 $\mu$m with the content of LiCl from 0.1 to 5.0%. Meanwhile, when the LiCl content is below 0.5%, the distribution of the PVDF nanofibers is much narrower. When the LiCl content is higher than 1.0%, the diameter distribution of fibers gradually enlarges, and the variance of FD increases from 0.12 to 0.82 $\mu$m. When the LiCl content is 5.0%, it is very difficult to collect PVDF nanofibers, as most of the nanofibers gather around the electrospun tip. The reason maybe is that when excessive LiCl is added, the splitting of the micro/nanofibers is not significant in the jet instability area due to the


https://doi.org/10.1021/acsami.2c11251
ACS Appl. Mater. Interfaces 2022, 14, 39610−39621

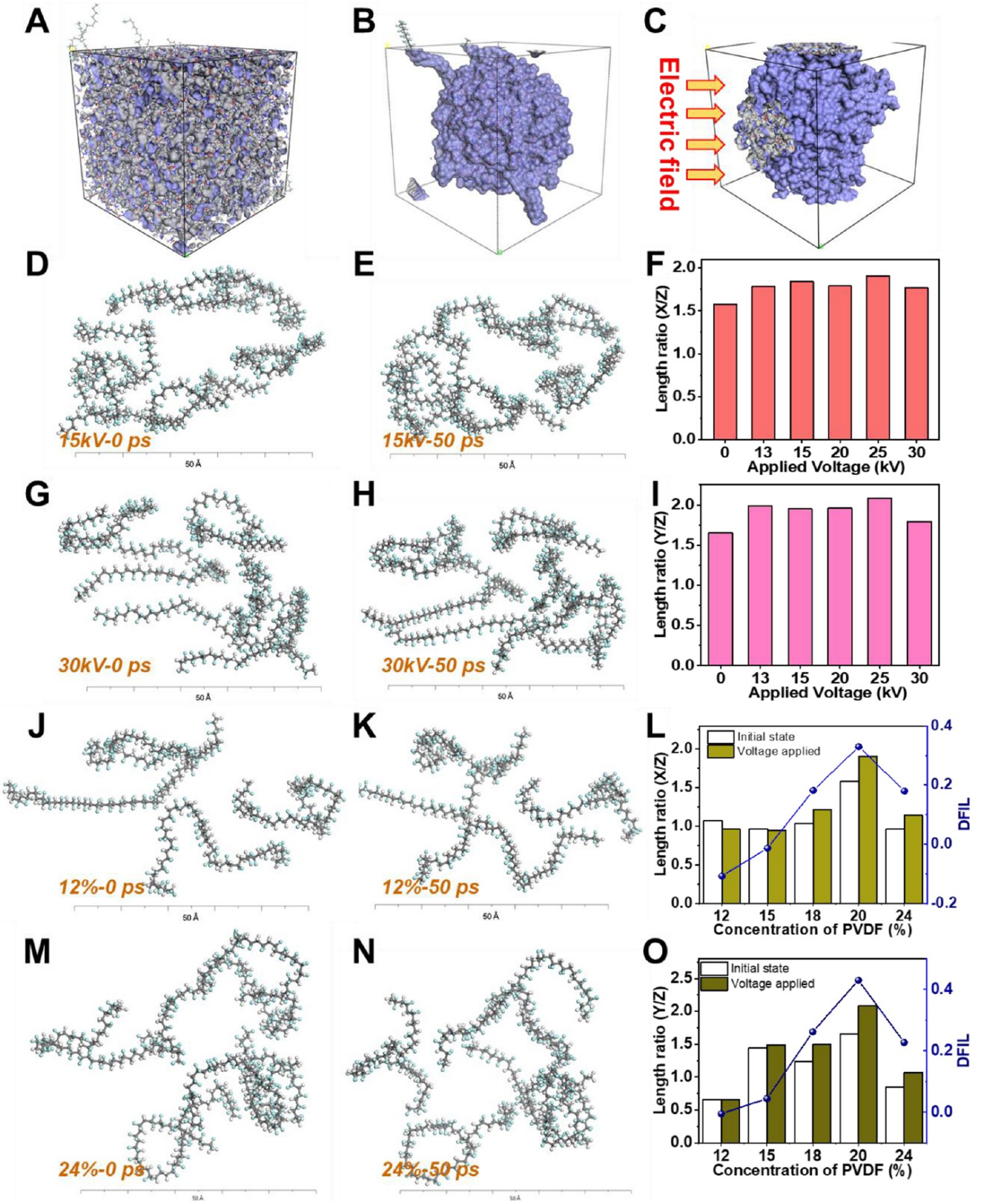


**Figure 4.** Molecular dynamics simulation of PVDF in DMF solvent under varying electric fields. (A) Original state of PVDF solution in a simulated cube with a size of 55 Å × 55 Å × 55 Å; (B) state of a drop of PVDF solution without an applied electric field; (C) state of a drop of PVDF solution with an applied electric field; (D, E) states of 20% PVDF in DMF at 0 and 50 ps under a voltage of 15 kV; (G, H) states of 20% PVDF in DMF at 0 and 50 ps under a voltage of 30 kV; (F, I) length ratio of X/Z and Y/Z, respectively, to 20% PVDF in DMF with varying voltage; (J, K) states of 12% PVDF in DMF at 0 and 50 ps under a voltage of 25 kV; (M, N) states of 24% PVDF in DMF at 0 and 50 ps under a voltage of 25 kV; (L, O) length ratio of X/Z, Y/Z, and DFIL to different concentrations of PVDF under a voltage of 25 kV.



https://doi.org/10.1021/acsami.2c11251
ACS Appl. Mater. Interfaces 2022, 14, 39610−39621

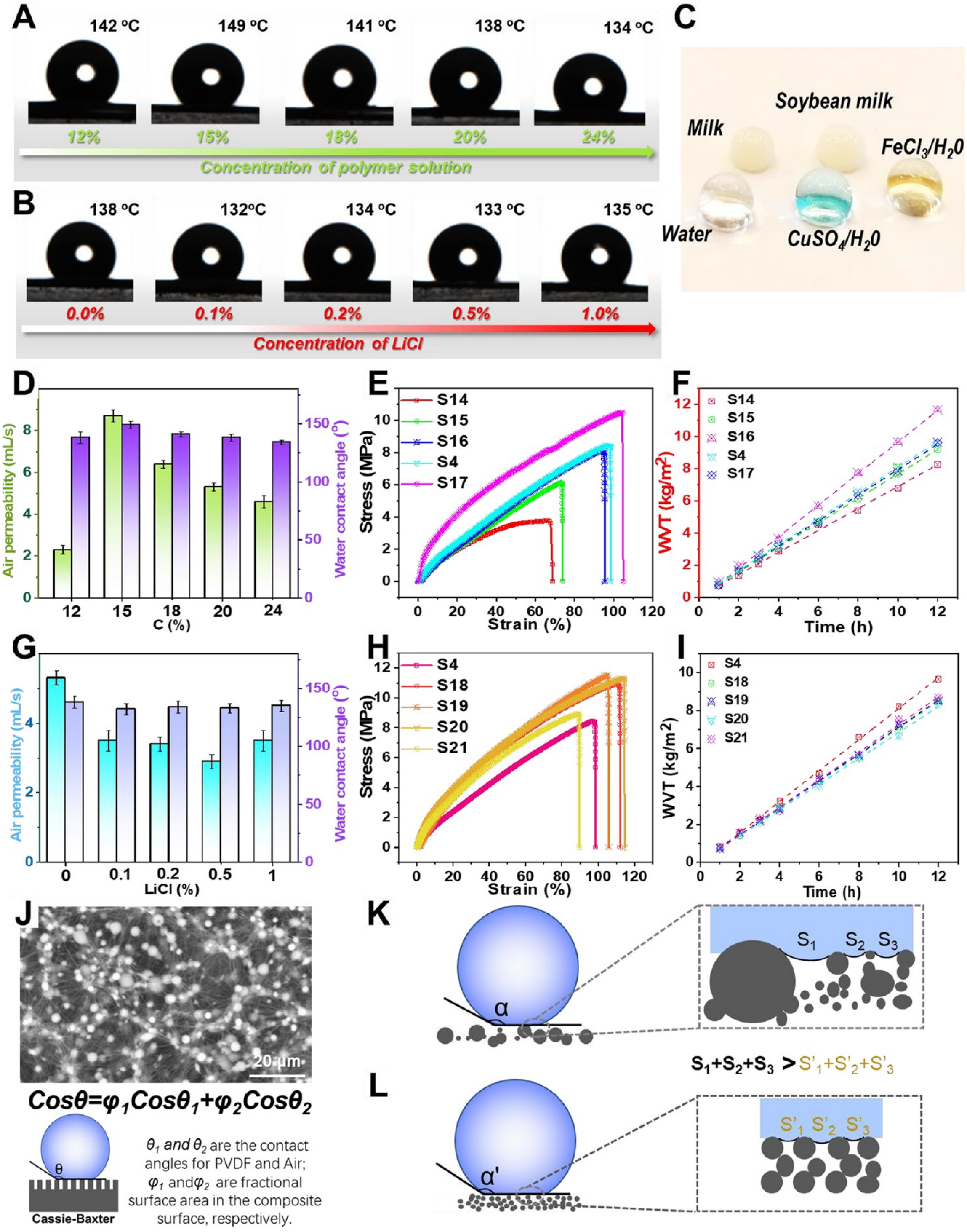

Figure 5. Performances of representative electrospun membranes with different microstructures. (A, B) Optical photographs of WCA of samples fabricated via different polymer concentrations and LiCl. (C) Different liquid drops on the sample with structured microbeads. (D−F) AP, WVTR, WVC, and mechanical properties of various samples fabricated via different polymer concentrations. (G−I) AP, WVTR, WVC, and mechanical properties of various samples fabricated via different contents of LiCl. (J) SEM picture of the microbead-based sample and the theory of the Cassie−Baxter model. (K, L) Schematical diagrams of contact areas to electrospun membranes with microbeads and fine nanofibers.

excellent conductivity of the polymer solution. So, the diameter of the prepared nanofiber is bigger when a large amount of LiCl is added.

Furthermore, we meticulously designed and simulated the electrospinning process of PVDF. Specifically, the morphological change of PVDF droplets under the action of an electric field was theoretically investigated via dynamic molecule simulation as shown in Figure 4. First, the original molecule state of PVDF in DMF was built in a cube with the size of 55 Å × 55 Å × 55 Å, and the deformation of the droplet was then investigated under varying applied electric fields, as shown in Figure 4A−C. Specific simulating processes and results were provided (Figure 4D−I, Figure S6, and Video S1). The simulated states of the PVDF chain in varying electric voltage



https://doi.org/10.1021/acsami.2c11251
ACS Appl. Mater. Interfaces 2022, 14, 39610−39621

from 0 to 30 kV were investigated, and the result of length ratio $X/Z$ and $Y/Z$ shows a great different change in Figures 4F, I. The length ratio of $X/Z$ increase from approximately 1.57 to 1.90 with the increase in applied voltage, while the value of $Y/Z$ increase from 1.65 to 2.08. However, the length ratio of $X/Y$ has a neglectable change (Figure S6). Results indicate that droplets of PVDF undergo severe traction deformation driven by a high electric field, thereby increasing applied voltage can promote the formation of electrospinning jets. Moreover, we also simulated the effect of the concentration of the polymeric solution on the droplet morphology under the fixed electrostatic field (Figure 4J−O, Figure S7, and Video S2). The results show that the degree of the droplet deformation affected by the polymer concentration is significant. With the increase of the polymer concentration from 12 to 24%, the difference value between the final state and initial state of the length ratio (DFIL) of $X/Z$ and $Y/Z$ increases in Figure 4L, O. The different values of the length ratio of $X/Z$ and $Y/Z$ is up to 0.33 and 0.43 at the concentration of 20% PVDF, meaning that when the concentration over 20% the tensile deformation of polymer droplets under electric field becomes significant. This favors the electrospinning process, a corresponding experimental phenomenon that microbeads become less when the concentration of PVDF solution surpasses 20% as shown in Figure 3K. To sum up, we simulated and defined the deformation of PVDF droplets in different directions under the action of a high electric field, and the corresponding simulation and experimental phenomena showed a good matching, which well explained the morphological changes in the droplets and the morphologies of electrospun fibers in the electric field under different conditions.

**3.2. Effects of Micro/Nanomorphologies on Performances of Electrospun Membranes.** Performances of fabricated electrospun membranes, such as mechanical properties, moisture permeabilities, air permeabilities, and so forth, affected by micro/nanomorphologies were investigated and analyzed in detail. Significant differences in morphologies, meaning the diameter of fibers and the morphology of microbeads can be controlled by factors of polymer concentration and the content of LiCl. So, in this section, we mainly focus on the relationship between the properties of electrospun membranes and these two factors. The performance of several samples with representative structures, specifically, samples including S4 and S14−21 were used, and the specific parameters for preparing these samples were provided in Table S1. First, the molecule structures and elements of the fabricated membrane were confirmed by FT-IR and element mapping (Figures S8 and S9). Specifically, the peak at 1182 $cm^{-1}$ was assigned to the C−F stretching and the peak at 1401 $cm^{-1}$ was assigned to C−H deformation.[56] The element mapping demonstrates the membrane mainly contains two elements, fluorine, and carbon. Therefore, the PVDF in the membrane was confirmed.

In comparison with the WCA of different samples, membranes with structured microbeads show the highest WCA up to 151°; however, fine nanofiber-based membranes have a stable WCA between 132 and 138° as shown in Figure 5A, B. Therefore, by regulating microbeads and nanofibers, WCAs of membranes can be adjusted from 132 to 151°. The excellent hydrophobicity of the electrospun membrane was demonstrated in Figure 5C. At the same time, we compared the other properties, like air permeability, tensile stress, and water vapor transmission rate of samples with different structures (Figure 5D−I, Figures S10 and S11 and Table S2). Results revealed that nanomembranes with microbeads have better air permeability and higher water vapor transmission rate. The air permeability (AP) of the membrane is up to 8.7 mL/s when the polymer solution concentration is 15%, while the WVTR of the fibrous membrane can achieve up to 23106 g/($m^2$ day) when the polymer solution concentration is 18%. For comparison, the highest WVTR of all finer nanofiber-based membranes was at 17546 g/($m^2$ day), and membranes show AP values between 2.9 and 3.5 mL/s in Figures 5G−I. The reason why a microbead-based membrane with a relatively higher WVTR is very interesting and the mechanism of that are demonstrated in Figure 5J−L. The water contact angle of the fibrous membrane obeys the Cassie model in eq 2.[57]

$$\cos\theta = \varphi_1\cos\theta_1 + \varphi_2\cos\theta_2 \tag{2}$$

Where $\theta_1$ and $\theta_2$ are the contact angles of PVDF and air. $\varphi_1$ and $\varphi_2$ are the fractional surface area in the rough surface, respectively.

Considering an ideal state of the contact angle between air and water, $\theta_2 = 180°$, and the total $\varphi_1 + \varphi_2 = 1$, eq 2 can be transferred to the Cassie−Baxter model in eq 3.[58]

$$\cos\theta = \varphi_1(1 + \cos\theta_1) - 1 \tag{3}$$

High roughness means that the contacting interface between materials and water decreases, so the value of $\varphi_1$ decreases. Thereby, the contact angle of the water droplet increases. The roughness of the membrane increases with the containing of microbeads. Figure 5K, L shows schematic diagrams that the higher roughness of the membrane favors the higher contact of air with the water, and thus the transpiration of water is effectively promoted. So, we observed that the fibrous membrane with microbeads, such as S4, displays higher WVTR compared to membranes with fine nanofibers. The air permeability and moisture permeability of the prepared fibrous membrane also drops via adding different contents of LiCl, which is because the FD becomes smaller compared with others. Of note, when the LiCl content is 0.5%, the air permeability of the prepared membrane is the lowest at 2.9 mL/s; by comparison, that of S4 with microbeads can reach up to 5.3 mL/s. The mechanical properties of microbead-based membranes display a lower level when compared with finer nanofiber-based membranes. In detail, since the addition of LiCl facilitate the formation of the fine nanofiber, the mechanical property of the nanomembrane without microbeads are well improved compared with the normal S4 with microbeads. The broken strength of S4 is 8.4 MPa while that of the perfect nanofiber with LiCl reaches up to 11.5 MPa, meaning this performance has been enhanced 1.4 times only by adding tiny amounts of inorganic salts (Figure 5H and Figure S11). It should be noted that when the content of LiCl increases above 0.5%, the mechanical property of the as-prepared PVDF-based nanomembrane shows a decreasing trend. The reason is that the excessive addition of LiCl may lead to defects inside nanofibers, and thus the overall mechanical property of fibrous membrane deteriorates.

Overall, although the air permeability and the water vapor transmission rate of the microbead-based membrane are relatively higher, the mechanical property of the membrane containing microbeads is very poor. Therefore, the practical application of the membrane with microbeads is limited. It is of great significance to prepare fibrous membranes integrated with the advantages of microbeads and nanofibers. In the following section, the construction of membranes with structured

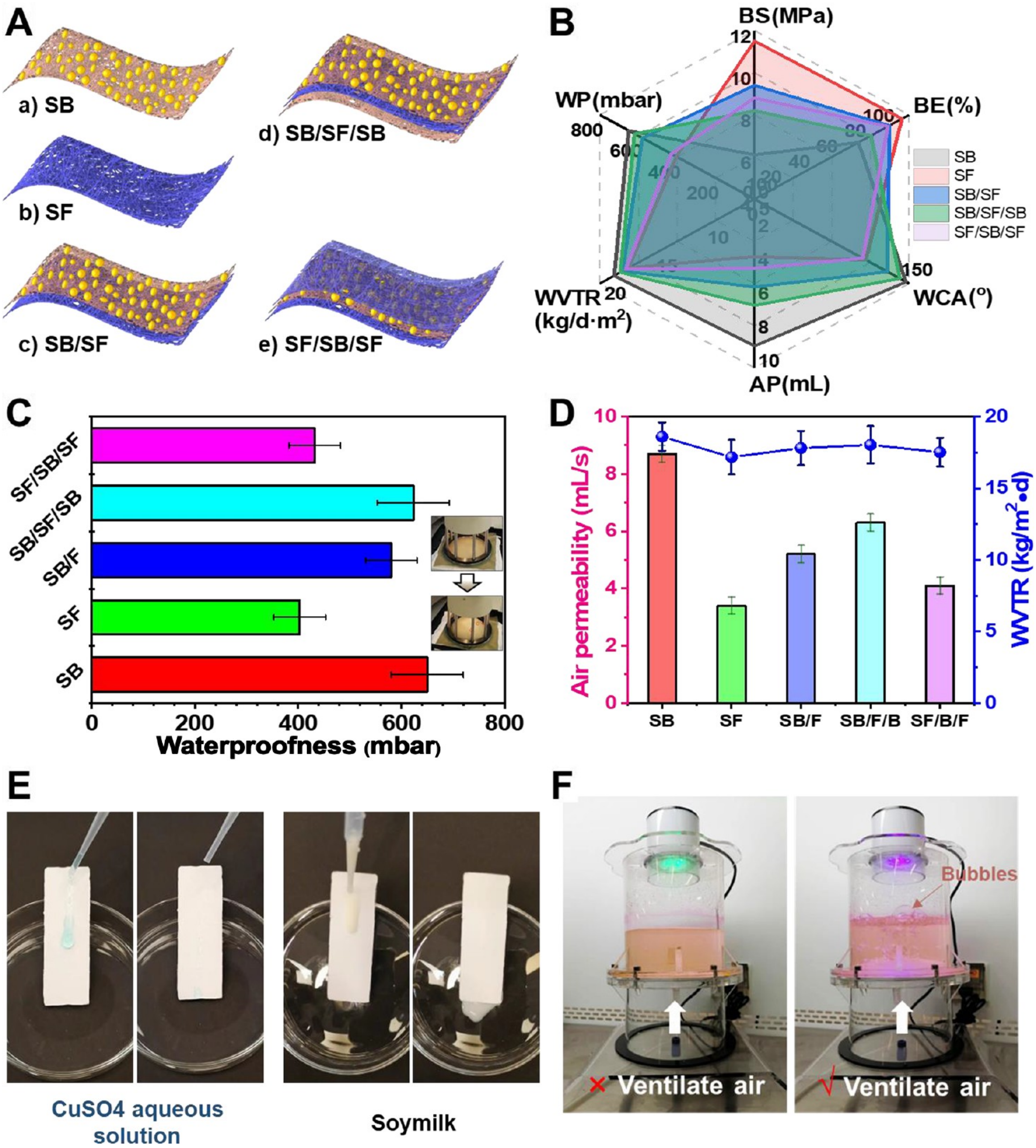


**Figure 6.** Comprehensive properties of fibrous membranes with structured microbeads/nanofibers. (A) Design of fibrous membranes with structured microbeads/nanofibers and sublayers. (B) Comprehensive properties of structured electrospun membranes. (C, D) Properties, such as waterproofness, water contact angle, air permeability, and water vapor transmission rate of diversely designed membranes. (E) Demonstration of superhydrophobicity of fabricated membranes. (F) Demonstration of waterproofness and breathability of the fibrous membrane.

microbeads and nanofibers has been focused on and systematically investigated.

**3.3. Comprehensive Properties of Structured Electrospun Membranes.** As the mechanical property is fundamental to materials, the sample with microbeads (SB) is not suitable for many practical applications. Meanwhile, the sample with fine nanofibers (SF) has a lower WVTR, WCA, and AP as prepared nanofibers are thinner and more uniform, its application is also limited in the fields of smart fabrics, intelligent protection, and wearable devices. Therefore, it is crucial to design membranes with structured microbeads and nanofibers, realizing adjustable comprehensive properties via constructing structured sublayers. Based on the above investigation, structured microbeads/nanofibers membranes with programmable layers were fabricated via controllable electrospinning. The controlling parameters and formulas used to fabricate structured electrospun membranes were provided in Table1. Comprehensive properties of fibrous membranes were investigated and compared (Figure 6, Table 2, **and** Figure S12). By comparison (Table S3), fibrous nanomembranes with dual-layer and triple-layer micro/nanostructures demonstrate better comprehensive properties, with a high WVTR > 17500 g/(m$^2$ day), a high AP > 5 mL/s, and a large WCA up to 151°, good tensile strength of 9.4 MPa, and high hydrostatic pressure of 623 mbar, enabling a wider service range of electrospun membrane.

Specifically, five types of structured microbead/nanofiber membranes with different features were constructed as shown in Figure 6A. Single-layer membranes include the typical microbead-based membrane (SB) and the perfect nanofiber-based membrane (SF); the dual-layer membrane is the integrated


https://doi.org/10.1021/acsami.2c11251
ACS Appl. Mater. Interfaces 2022, 14, 39610−39621

**Table 2. Comprehensive Properties of Structured Electrospun Membranes[a]**

| P / S | BS (MPa) | BE (%) | WCA (o) | AP (mL/s) | WVTR (g/m2 ·d) | WP (mbar) |
|---|---|---|---|---|---|---|
| SB | 6.1 | 74 | 149±5 | 8.7±0.3 | 18602 | 650 |
| SF | 11.5 | 105 | 136±3 | 3.4±0.3 | 17175 | 402 |
| SB/SF | 9.4 | 96 | 143±5 | 5.2±0.3 | 17805 | 580 |
| SB/SF/SB | 8.2 | 83 | 147±5 | 6.3±0.3 | 18036 | 623 |
| SF/SB/SF | 8.8 | 95 | 134±3 | 4.1±0.3 | 17518 | 432 |

[a]P, controlling parameters; S, samples; BS, broken stress; BE, broken elongation; SB, sample with microbeads; SF, sample with all fine nanofibers; SB/SF, sample with a half layer of a microbead-based membrane and a half layer of a fine nanofiber-based membrane; SB/SF/SB, sample with a sandwich structure where the middle is a nanofiber-based layer and the two outside layers are microbead-based; SF/SB/SF, sample with a sandwich structure where the middle is a microbead-based layer and the two outside layers are nanofiber-based.

membrane SB/SF composed of half microbead-based layer and half perfect nanofiber membrane; two types of three-layer membranes are the membrane with SF as the interlayer SB as outer layers, and the membrane with SB as the interlayer SF as outer layers, respectively. Their essential properties including mechanical properties, the water contact angle, the air permeability, the water vapor transmission rate, and the hydrostatic pressure, are shown in the radar map of Figure 6B. In comparison, two-layer and three-layer integrated membranes, in particular SB/SF and SB/SF/SB, have broader service spaces. Designed two-layer and three-layer structured membranes not only have the adjusting bigger water contact angle and higher air permeability but also have high moisture permeability and good mechanical strength. Thus, integrated membranes display excellent comprehensive properties. It is worth mentioning that the reduction of the hydrostatic pressure resistance of SB/SF and SB/SF/SB is neglectable compared with the best membrane of SB as shown in Figure 6C. Meanwhile, as illustrated in Figure 6D, compared with SF, the AP values of SB/SF and SB/SF/SB improve 52 and 85%, respectively. The excellent hydrophobicity of the fabricated membrane was demonstrated in Figure 6E, showing that no obvious attached liquids on the membrane when liquids flow down on it. Demonstrations of the good air permeability and the hydrostatic pressure of the structured membranes were given (Figure 6F, Figure S12, and Video S3). In the following research, we plan to use an industrial-scale electrospinning system for industrialization and large-scale preparation of the structured micro-/nanomembrane. The study in this paper based on needle electrospinning technology and related formulation optimization will provide significant guidance in the technology transformation to needleless electrospinning.

To sum up, through the regulation of electrospinning microbeads and nanofibers as well as the construction of structured sublayers of fibrous membranes, we effectively fabricated diverse structured fibrous membranes with tunable comprehensive properties. These membranes can be used in diverse applications, such as waterproof breathable areas, soft electronics, and intelligent wearables. Meanwhile, these approaches to controlling morphologies of microbeads and nanofibers and to constructing secondary interlayer structures play a good guiding role in materials science and technology.

## 4. CONCLUSION

In this study, a lotus leaf-inspired electrospun membrane on a large scale with good comprehensive properties was systematically designed, prepared, and evaluated. The micro/nanostructures of the structured membrane in terms of microbeads and nanofibers were quantitatively analyzed and meticulously simulated over various control parameters, including V, Toc, FS, C, and LiCl in detail. Experimental results of electrospinning and molecular dynamics simulations of polymeric droplets show a good match. Based on the controllable fabrication of microbeads and nanofibers, comprehensive properties, such as the BS, BE, AP, WVTR, and WP of the prepared membranes with controllable micro/nanomorphologies and sublayers were systematically achieved, investigated, and optimized. Inspired by the biomimetic concept of the lotus leaf, this research created a good designability of the electrospun membrane in terms of microbeads and nanofibers as well as sublayer structures. In comparison, structured membranes with dual layers and triple layers of regulated micro/nanostructures demonstrate better comprehensive performances. Prepared lotus leaf-inspired membranes have high performance in AP and WVTR, while they are also equipped with good mechanical properties. Therefore, designed SB/SF and SB/SF/SB have wider service ranges. It is worth mentioning that these membranes have a large WCA up to 151°, AP > 5 mL/s, WVTR > 17 500 g/($m^2$ day), and WP > 580 mbar. This study provides a feasible approach to constructing fibrous membranes that can optimize comprehensive properties, enabling them to be used as advanced filtration, waterproof-breathable devices, flexible electronics, intelligent wearables, etc. We believe that this article is of great significance in the development of nanomaterials and electrospinning technologies.

## ■ ASSOCIATED CONTENT

### Supporting Information

The Supporting Information is available free of charge at https://pubs.acs.org/doi/10.1021/acsami.2c11251.

Micro/nanostructures, molecule dynamics simulation, FT-IR spectra, EDS element mapping, tensile strength, waterproofness of structured electrospun membrane (PDF)



https://doi.org/10.1021/acsami.2c11251
ACS Appl. Mater. Interfaces 2022, 14, 39610−39621

Video S1, states of 20% PVDF at 0 and 50 ps under 30 kV (AVI)

Video S2, states of 24% PVDF at 0 and 50 ps under 25 kV (AVI)

Video S3, demonstration of the waterproof breathable function (MP4)

## ■ AUTHOR INFORMATION


### Corresponding Author

**Jinlian Hu** − *Department of Biomedical Engineering, City University of Hong Kong, Hong Kong S.A.R 999077, China; City University of Hong Kong Shenzhen Research Institute, Shenzhen 518057, P. R. China;* orcid.org/0000-0001-8914-5473; Email: jinliahu@cityu.edu.hk

### Authors

**Shuo Shi** − *Department of Biomedical Engineering, City University of Hong Kong, Hong Kong S.A.R 999077, China*

**Chuanwei Zhi** − *Department of Biomedical Engineering, City University of Hong Kong, Hong Kong S.A.R 999077, China*

**Shuai Zhang** − *Department of Biomedical Engineering, City University of Hong Kong, Hong Kong S.A.R 999077, China*

**Jieqiong Yang** − *Department of Biomedical Engineering, City University of Hong Kong, Hong Kong S.A.R 999077, China*

**Yifan Si** − *Department of Biomedical Engineering, City University of Hong Kong, Hong Kong S.A.R 999077, China*

**Yuanzhang Jiang** − *College of Biomass Science and Engineering, Key Laboratory of Leather Chemistry and Engineering of Ministry of Education, Sichuan University, Chengdu 610065, China;* orcid.org/0000-0003-2501-9712

**Yang Ming** − *Institute of Textiles and Clothing, The Hong Kong Polytechnic University, Hong Kong S.A.R 999077, China*

**Kin-tak Lau** − *School of Engineering, Swinburne University of Technology, Melbourne, Victoria 3122, Australia*

**Bin Fei** − *Institute of Textiles and Clothing, The Hong Kong Polytechnic University, Hong Kong S.A.R 999077, China;* orcid.org/0000-0002-4274-1873

Complete contact information is available at: https://pubs.acs.org/10.1021/acsami.2c11251


### Author Contributions

J.H. and S.S. conceived the concept together. J.H. supervised the whole project throughout, including the writing up and final proofing of the manuscript. In addition to the concept development, S.S. and C.Z. conducted the main experimental design and drafted the manuscript. S.Z. investigated the dynamic molecule simulation of electrospun process; J.Y., Y.S., Y.J., and Y.M. helped with some tests. K.-t.. and B.F.revised the manuscript and provided some facilities for conducting experiments.

### Notes

The authors declare no competing financial interest.

## ■ ACKNOWLEDGMENTS


The authors gratefully acknowledge the financial support from the Startup Grant of CityU ("Laboratory of Wearable Materials for Healthcare", Grant 9380116), National Natural Science Foundation of China ("Study of high performance fiber to be achieved by mimicking the hierarchical structure of spider-silk", Grant 52073241; "Study of Multi-Responsive Shape Memory Polyurethane Nanocomposites Inspired by Natural Fibers", Grant 51673162; "Developing Spider-Silk-Model Artificial Fibers by A Chemical Synthetic Approach", Grant 15201719), and the Contract Research ("Development of Breathable Fabrics with Nano-Electrospun Membrane", CityU ref.: 9231419).


## ■ REFERENCES


(1) Shi, S.; Si, Y.; Han, Y.; Wu, T.; Iqbal, M. I.; Fei, B.; Li, R. K.; Hu, J.; Qu, J. Recent Progress in Protective Membranes Fabricated via Electrospinning: Advanced Materials, Biomimetic Structures, and Functional Applications. *Adv. Mater.* **2021**, 2107938.

(2) Jiang, L.; Zhao, Y.; Zhai, J. A Lotus-leaf-like Superhydrophobic Surface: a Porous Microsphere/nanofiber Composite Film Prepared by Electrohydrodynamics. *Angew. Chem., Int. Ed.* **2004**, *116*, 4438−4441.

(3) Zhan, H.-J.; Wu, K.-J.; Hu, Y.-L.; Liu, J.-W.; Li, H.; Guo, X.; Xu, J.; Yang, Y.; Yu, Z.-L.; Gao, H.-L.; Luo, X.-S.; Chen, J.-F.; Ni, Y.; Yu, S.-H. Biomimetic Carbon Tube Aerogel Enables Super-elasticity and Thermal Insulation. *Chem.* **2019**, *5*, 1871−1882.

(4) Lee, S.-M.; Pippel, E.; Gösele, U.; Dresbach, C.; Qin, Y.; Chandran, C. V.; Bräuniger, T.; Hause, G.; Knez, M. Greatly Increased Toughness of Infiltrated Spider Silk. *Science* **2009**, *324*, 488−492.

(5) Gu, L.; Jiang, Y.; Hu, J. Scalable Spider-Silk-Like Supertough Fibers using a Pseudoprotein Polymer. *Adv. Mater.* **2019**, *31*, 1904311.

(6) Wang, X.; Ding, B.; Li, B. Biomimetic Electrospun Nanofibrous Structures for Tissue Engineering. *Mater. Today* **2013**, *16*, 229−241.

(7) Xue, J.; Wu, T.; Dai, Y.; Xia, Y. Electrospinning and Electrospun Nanofibers: Methods, Materials, and applications. *Chem. Rev.* **2019**, *119*, 5298−5415.

(8) Ji, D.; Fan, L.; Li, L.; Peng, S.; Yu, D.; Song, J.; Ramakrishna, S.; Guo, S. Atomically Transition Metals on Self-supported Porous Carbon Flake Arrays as Binder-free Air Cathode for Wearable Zinc− air Batteries. *Adv. Mater.* **2019**, *31*, 1808267.

(9) Gugliuzza, A.; Drioli, E. A Review on Membrane Engineering for Innovation in Eearable Fabrics and Protective Textiles. *J. Membr. Sci.* **2013**, *446*, 350−375.

(10) Chen, L.; Wu, F.; Li, Y.; Wang, Y.; Si, L.; Lee, K. I.; Fei, B. Robust and Elastic Superhydrophobic Breathable Fibrous Membrane with In Situ Grown Hierarchical Structures. *J. Membr. Sci.* **2018**, *547*, 93−98.

(11) Gibson, P.; Schreuder-Gibson, H.; Pentheny, C. Electrospinning Technology: Direct Application of Tailorable Ultrathin Membranes. *J. Coat. Fabr.* **1998**, *28*, 63−72.

(12) Hu, J.; Wu, Y.; Zhang, C.; Tang, B. Z.; Chen, S. Self-adaptive Water Vapor Permeability and its Hydrogen Bonding Switches of Bio-inspired Polymer Thin Films. *Chen, Mater. Chem. Front.* **2017**, *1*, 2027−2030.

(13) Shi, S.; Han, Y.; Hu, J. Robust Waterproof and Self-adaptive Breathable Membrane with Heat Retention Property for Intelligent Protective Cloth. *Prog. Org. Coat.* **2019**, *137*, 105303.

(14) Shi, S.; Zhu, K.; Chen, X.; Hu, J.; Zhang, L. Cross-linked Cellulose Membranes with Robust Mechanical Property, Self-adaptive Breathability, and Excellent Biocompatibility. *ACS Sustainable Chem. Eng.* **2019**, *7*, 19799−19806.

(15) *Protective Clothing Market Size, Share & Industry Analysis, By Product (Disposable and Durable), By Application (Flame Retardant Apparel, Chemical Defending Garment {Radiation Protection, Particulate Matter, and Others}, Clean Room Clothing, Mechanical Protective Clothing, and Others), By End-Use (Pharmaceutical, Oil & Gas, Chemical, Firefighters, and Others), and Regional Forecase, 2020−2027*; Fortune Business Insights, 2020.https://www.fortunebusinessinsights.com/protective-clothing-market-102707.

(16) Verbeek, J. H.; Rajamaki, B.; Ijaz, S.; Sauni, R.; Toomey, E.; Blackwood, B.; Tikka, C.; Ruotsalainen, J. H.; Balci, F. S. K. Personal Protective Equipment for Preventing Highly Infectious Diseases due to Exposure to Contaminated Body Fluids in Healthcare Staff. *Cochrane Database Syst. Rev.* **2020**, *4*, CD011621.

(17) Rodriguez-Palacios, A.; Cominelli, F.; Basson, A. R.; Pizarro, T. T.; Ilic, S. Textile Masks and Surface Covers-a Spray Simulation Method and a "Universal Droplet Reduction Model" Against Respiratory Pandemics. *Front. Med.* **2020**, *7*, 260.

(18) Husain, S. A.; Husain, S. A.; Khan, O. U.; D'Cruz, L.; Allgar, V. Review of Hygiene Adaptations Among UK Doctors in Controlling the Spread of Sars-Cov-2 Infection. *Clin. Med.* **2021**, *21*, e20.

(19) Deng, W.; Sun, Y.; Yao, X.; Subramanian, K.; Ling, C.; Wang, H.; Chopra, S. S.; Xu, B. B.; Wang, J. X.; Chen, J. F.; et al. Masks for COVID-19. *Adv. Sci.* **2022**, *9*, 2102189.

(20) Liu, R.; Ji, D.; Zhou, G.; Liu, Z.; Xu, Q.; Ramakrishna, S. Electrospun Nanofibers for Personal Protection in Mines. *Chem. Eng. J.* **2021**, *404*, 126558.

(21) Zhu, K.; Shi, S.; Cao, Y.; Lu, A.; Hu, J.; Zhang, L. Robust Chitin Films with Good Biocompatibility and Breathable Properties. *Carbohydr. Polym.* **2019**, *212*, 361−367.

(22) Han, Y.; Jiang, Y.; Hu, J. Collagen Incorporation Into Waterborne Polyurethane Improves Breathability, Mechanical Property, and Self-Healing Ability. *Composites, Part A* **2020**, *133*, 105854.

(23) Zhou, W.; Gong, X.; Li, Y.; Si, Y.; Zhang, S.; Yu, J.; Ding, B. Environmentally Friendly Waterborne Polyurethane Nanofibrous Membranes by Emulsion Electrospinning for Waterproof and Breathable Textiles. *Chem. Eng. J.* **2022**, *427*, 130925.

(24) Miao, D.; Wang, X.; Yu, J.; Ding, B. A Biomimetic Transpiration Textile for Highly Efficient Personal Drying and Cooling. *Adv. Funct. Mater.* **2021**, *31*, 2008705.

(25) Williams, J. T. *Waterproof and Water Repellent Textiles and Clothing*; Woodhead Publishing, 2017.

(26) Hu, J.; Chen, S. A Review of Actively Moving Polymers in Textile Applications. *J. Mater. Chem.* **2010**, *20*, 3346−3355.

(27) Hu, J. The Use of Smart Materials in Cold Weather Apparel. In *Textiles for Cold Weather Apparel*; Elsevier, 2009; pp 84−112.

(28) Si, Y.; Chen, L.; Yang, F.; Guo, F.; Guo, Z. Stable Janus Superhydrophilic/Hydrophobic Nickel Foam for Directional Water Transport. *J. Colloid Interface Sci.* **2018**, *509*, 346−352.

(29) Yu, N.; Zhu, X.; Feng, S.; Zhang, C.; Liu, L.; Ju, S.; Zhong, Z.; Xing, W. A Breathable PTFE Membrane for Enhanced Moxibustion Process and Occupational Health Protection. *J. Membr. Sci.* **2022**, *655*, 120579.

(30) Midha, V. K.; Dakuri, A.; Midha, V. Studies on the Properties of Nonwoven Surgical Gowns. *J. Ind. Text.* **2013**, *43*, 174−190.

(31) Rengasamy, R. S.; Kothari, V. K.; Bele, V. S.; Khanna, R. Liquid Sorption Behaviour of Nonwovens. *J. Text. Inst.* **2011**, *102*, 1019−1030.

(32) Hao, X.; Zhang, J.; Guo, Y.; Zhang, H. Studies on Porous and Morphological Structures of Expanded PTFE Membrane Through Biaxial Stretching Technique. *Int. Nonwovens J.* **2005**, *2*, DOI: 10.1177/1558925005os-1400205.

(33) Abeykoon, C.; McMillan, A.; Nguyen, B. K. Energy Efficiency in Extrusion-Related Polymer Processing: A Review of State of the Art and Potential Efficiency Improvements. *Renew. Sustain. Energy Rev.* **2021**, *147*, 111219.

(34) Patel, S.; Xanthos, M. Environmental Issues in Polymer Processing: A Review on Volatile Emissions and Material/Energy Recovery Options. *Adv. Polym. Technol.* **2001**, *20*, 22−41.

(35) Ebnesajjad, S. *Expanded PTFE Applications Handbook: Technology, Manufacturing and Applications*; William Andrew, 2016.

(36) Kim, C.; Yang, K. Electrochemical Properties of Carbon Nanofiber Web as an Electrode for Supercapacitor Prepared by Electrospinning. *Appl. Phys. Lett.* **2003**, *83*, 1216−1218.

(37) He, G.; Cai, Y.; Zhao, Y.; Wang, X.; Lai, C.; Xi, M.; Zhu, Z.; Fong, H. Electrospun Anatase-Phase TIO2 Nanofibers with Different Morphological Structures and Specific Surface Areas. *J. Colloid Interface Sci.* **2013**, *398*, 103−111.

(38) Sun, X.; Bai, L.; Li, J.; Huang, L.; Sun, H.; Gao, X. Robust Preparation of Flexibly Super-Hydrophobic Carbon Fiber Membrane by Electrospinning for Efficient Oil-Water Separation in Harsh Environments. *Carbon* **2021**, *182*, 11−22.

(39) Wang, X.; Ding, B.; Yu, J.; Wang, M. Engineering Biomimetic Superhydrophobic Surfaces of Electrospun Nanomaterials. *Nano today* **2011**, *6*, 510−530.

(40) Garkal, A.; Kulkarni, D.; Musale, S.; Mehta, T.; Giram, P. Electrospinning Nanofiber Technology: A Multifaceted Paradigm in Biomedical Applications. *New J. Chem.* **2021**, *45*, 21508−21533.

(41) Yu, X.; Li, Y.; Wang, X.; Si, Y.; Yu, J.; Ding, B. Thermoconductive, Moisture-Permeable, and Superhydrophobic Nanofibrous Membranes with Interpenetrated Boron Nitride Network for Personal Cooling Fabrics. *ACS Appl. Mater. Interfaces* **2020**, *12*, 32078−32089.

(42) Zhou, W.; Yu, X.; Li, Y.; Jiao, W.; Si, Y.; Yu, J.; Ding, B. Green-Solvent-Processed Fibrous Membranes with Water/Oil/Dust-Resistant and Breathable Performances for Protective Textiles. *ACS Appl. Mater. Interfaces* **2021**, *13*, 2081−2090.

(43) Li, P.; Feng, Q.; Chen, L.; Zhao, J.; Lei, F.; Yu, H.; Yi, N.; Gan, F.; Han, S.; Wang, L.; Wang, X. Environmentally Friendly, Durably Waterproof, and Highly Breathable Fibrous Fabrics Prepared by One-Step Fluorine-Free Waterborne Coating. *ACS Appl. Mater. Interfaces* **2022**, *14*, 8613−8622.

(44) Zhang, S.; Liu, H.; Tang, N.; Zhou, S.; Yu, J.; Ding, B. Spider-Web-Inspired PM0. 3 Filters Based on Self-Sustained Electrostatic Nanostructured Networks. *Adv. Mater.* **2020**, *32*, 2002361.

(45) Zhao, J.; Zhu, W.; Wang, X.; Liu, L.; Yu, J.; Ding, B. Fluorine-Free Waterborne Coating for Environmentally Friendly, Robustly Water-Resistant, and Highly Breathable Fibrous Textiles. *ACS Nano* **2020**, *14*, 1045−1054.

(46) Zhao, J.; Wang, X.; Liu, L.; Yu, J.; Ding, B. Human Skin-Like, Robust Waterproof, and Highly Breathable Fibrous Membranes With Short Perfluorobutyl Chains for Eco-Friendly Protective Textiles. *ACS Appl. Mater. Interfaces* **2018**, *10*, 30887−30894.

(47) Guo, Y.; Zhou, W.; Wang, L.; Dong, Y.; Yu, J.; Li, X.; Ding, B. Stretchable PDMS Embedded Fibrous Membranes Based on an Ethanol Solvent System for Waterproof and Breathable Applications. *ACS Appl. Bio Mater.* **2019**, *2*, 5949−5956.

(48) Lendlein, A. Textiles Come to Life. *Mater. Today* **2008**, *11*, 59.

(49) Zhang, Q.; Li, Q.; Zhang, L.; Wang, S.; Harper, D. P.; Wu, Q.; Young, T. M. Preparation of Electrospun Nanofibrous Poly(Vinyl Alcohol)/Cellulose Nanocrystals Air Filter for Efficient Particulate Matter Removal with Repetitive Usage Capability via Facile Heat Treatment. *Chem. Eng. J.* **2020**, *399*, 125768.

(50) Patil, N. A.; Gore, P. M.; Jaya Prakash, N.; Govindaraj, P.; Yadav, R.; Verma, V.; Shanmugarajan, D.; Patil, S.; Kore, A.; Kandasubramanian, B. Needleless Electrospun Phytochemicals Encapsulated Nanofibre Based 3-Ply Biodegradable Mask for Combating COVID-19 Pandemic. *Chem. Eng. J.* **2021**, *416*, 129152.

(51) Shi, S.; Cui, M.; Sun, F.; Zhu, K.; Iqbal, M. I.; Chen, X.; Fei, B.; Li, R. K.; Xia, Q.; Hu, J. An Innovative Solvent-Responsive Coiling-Expanding Stent. *Adv. Mater.* **2021**, *33*, 2101005.

(52) Hou, D.; Yu, J.; Wang, P. Molecular Dynamics Modeling of the Structure, Dynamics, Energetics and Mechanical Properties of Cement-Polymer Nanocomposite. *Compos. B. Eng.* **2019**, *162*, 433−444.

(53) Li, Y.; Wang, S.; Wang, Q.; Xing, M. Enhancement of Fracture Properties of Polymer Composites Reinforced by Carbon Nanotubes: A Molecular Dynamics Study. *Carbon* **2018**, *129*, 504−509.

(54) Rafiei, S.; Maghsoodloo, S.; Saberi, M.; Lotfi, S.; Motaghitalab, V.; Noroozi, B.; Haghi, A. New Horizons in Modeling and Simulation of Electrospun Nanofibers: A Detailed Review. *Cellul. Chem. Technol.* **2014**, *48*, 401−424.

(55) Qin, X. H.; Yang, E. L.; Li, N.; Wang, S. Y. Effect of Different Salts on Electrospinning of Polyacrylonitrile (PAN) Polymer Solution. *J. Appl. Polym. Sci.* **2007**, *103*, 3865−3870.

(56) Elashmawi, I. Effect of LiCl Filler on the Structure and Morphology of PVDF Films. *Mater. Chem. Phys.* **2008**, *107*, 96−100.

(57) Yeh, K.-Y.; Chen, L.-J.; Chang, J.-Y. Contact Angle Hysteresis on Regular Pillar-Like Hydrophobic Surfaces. *Langmuir* **2008**, *24*, 245−251.

(58) Choi, W.; Tuteja, A.; Mabry, J. M.; Cohen, R. E.; McKinley, G. H. A Modified Cassie-Baxter Relationship to Explain Contact Angle Hysteresis and Anisotropy on Non-wetting Textured Surfaces. *J. Colloid Interface Sci.* **2009**, *339*, 208−216.